energies

MDPI

Article

Simplified Modeling and Analysis of Surface Temperature Distribution in Electrically Heated Catalyst for Diesel Urea-SCR Systems

Seoksu Moon [1,*], Sunhong Park [1], Jihyun Son [1], Kwangchul Oh [2] and Sungwook Jang [3]

[1] Department of Mechanical Engineering, Inha University, Incheon 22212, Korea
[2] Korea Automotive Technology Institute, Cheonan 31214, Korea
[3] Sejong R&D Center Co., Ltd., Yongin 16950, Korea
* Correspondence: ss.moon@inha.ac.kr

Abstract: Impending emission regulations of diesel engines for construction machineries would regulate nitrogen oxide emissions strictly in cold operating conditions. The urea-based selective catalytic reduction (urea-SCR) system coupled with the electrically heated catalyst (EHC) has been considered as a potential measure to meet the strict emission regulations by promoting evaporation and thermal decomposition of urea–water solution in cold operating conditions. Analyzing the thermal conditions in the EHC is crucial for the optimized operation and control of EHC-based urea-SCR systems under various engine operating conditions. In the current study, we introduce a simple one-dimensional analysis scheme to characterize the surface temperature distribution in the EHC based on energy conservation and the theories of forced internal convection. Since the EHC has a complicated internal structure with fine flow cells inside it, a flow cell in the EHC is extracted for the one-dimensional heat transfer analysis. EHC operation parameters such as exhaust gas flow rate and supplied electric power to the EHC are scaled to be applied for the flow cell analysis. The adequacy of the analysis scheme is then validated by surface temperature measurement results at the EHC outlet. The validation results showed over 95% prediction accuracy of the 1D analysis scheme in the operating conditions of a heavy-duty diesel engine. Based on proven reliability, the effects of geometric and operation parameters on the surface temperature distribution in the EHC were analyzed and discussed using the analysis results.

Keywords: selective catalytic reduction (SCR); electrically heated catalyst (EHC); surface temperature; convective heat transfer; forced internal convection; 1D modeling

Citation: Moon, S.; Park, S.; Son, J.; Oh, K.; Jang, S. Simplified Modeling and Analysis of Surface Temperature Distribution in Electrically Heated Catalyst for Diesel Urea-SCR Systems. *Energies* **2022**, *15*, 6406. https://doi.org/10.3390/en15176406

Academic Editor: Giorgio Vilardi

Received: 12 August 2022
Accepted: 30 August 2022
Published: 1 September 2022

1. Introduction

The reduction in exhaust gas emissions has become a critical issue in diesel engines due to environmental problems around the globe. Strict emission regulations are, therefore, imposed on diesel engines by many countries for passenger cars, trucks, marine machineries, and construction machineries. Particularly for construction machineries, in Europe and the U.S., Post Stage-V and Tier 5 regulations will be phased in, which would restrict NOx emissions strictly in cold operating conditions [1,2].

The urea-SCR system is one of the most popular after-treatment systems for the NOx reduction in diesel engines [3,4]. It injects the urea–water solution (normally composed of 32.5% urea and 67.5% water) into the exhaust gas and induces the evaporation and thermal decomposition of the urea–water solution by the thermal energy of the exhaust gas that forms ammonia (NH_3), as shown in Equation (1).

$$CO(NH_2)_2 + H_2O \rightarrow CO_2 + 2NH_3 \quad (1)$$

The ammonia can be used as the reduction agent of NOx so that the final emission products through the tailpipe can be nitrogen (N_2) and water (H_2O), as shown in Equations (2) and (3).

$$4NO + 4NH_3 + O_2 \rightarrow 4N_2 + 6H_2O \quad (2)$$

$$6NO_2 + 8NH_3 \rightarrow 7N_2 + 12H_2O \quad (3)$$

The evaporation and decomposition performance of the urea–water solution is affected by the atomization of urea–water sprays [4–6]. In conventional urea-SCR systems, advanced injection strategies and mixers have been widely employed to promote the atomization and local homogeneity of urea–water sprays [4–8]. On the other hand, the exhaust gas temperature is another critical factor affecting the evaporation and decomposition performance of urea–water sprays, which becomes inferior in cold operating conditions [9,10].

The EHC has been introduced as a measure to increase the operating temperatures of three-way catalysts (TWCs) in gasoline engines during the cold start [11–13]. It has also been applied to diesel oxidation catalysts (DOC) and urea-SCR systems to enhance the evaporation and decomposition performance of the urea–water solution, particularly in cold start conditions by increasing the exhaust gas temperature [14–17]. The evaporation and decomposition performance can be further enhanced by injecting the urea–water solution directly into the heater in the EHC so that the thermal energy of the heater can be used.

Considerable previous studies have investigated the chemical processes and temperature regimes associated with the evaporation, thermal decomposition, and undesired deposit formation of urea–water sprays for urea-SCR systems [18–27]. The evaporation of urea–water droplets can be initiated at 373 K, which is the saturation temperature of the water at the atmospheric pressure. The droplet evaporation time can become shorter upon the increase in surrounding gas temperature and the decrease in urea–water droplet size [18–21]. The thermal decomposition of urea can be initiated at a temperature over 410 K and forms the biuret and cyanuric acid in order based on the progress of decomposition [18–24]. The completion temperature of urea decomposition varies based on the residence time of the feed gas stream. For example, the complete thermal decomposition of urea can be achieved at the temperature of around 623 K when the residence time of the feed gas stream is 0.1 s [24]. The formation of urea deposits is governed by the wall film temperature and urea concentration of the urea–water solution. The composition of urea deposits varies with the wall film temperature based on the progress of thermal decomposition [25–27].

The results of previous fundamental studies can be referred to for the optimized design and control of EHC-based urea-SCR systems in various operating conditions such as exhaust gas temperature and flow rate, and electric power supplied to the heater. To accomplish the complete evaporation and decomposition of urea–water solution without the formation of a urea deposit, the thermal conditions in the EHC such as surface temperature and exhaust gas temperature distribution should be characterized first so that the accumulated knowledge of previous studies can be linked and used for the optimization of EHC-based urea-SCR systems. Particularly for the urea-SCR system adopting the direct injection of a urea–water solution to the EHC, the surface temperature distribution of the EHC becomes the most critical factor that must be characterized.

Figure 1 illustrates the structure of the EHC-based urea-SCR system which injects the urea–water solution directly into the heater. The EHC has a circular outer shape and contains a bundle of thin corrugated heater foils. The heater foils are rolled and stacked to maximize the effective area of heat transfer between the heater and exhaust gas which forms the fine flow cells inside the EHC. The size and structure of flow cells determine the flow conditions and convective heat transfer between the heater surface and exhaust gas, which in turn determine the heater surface temperature and outflowing exhaust gas temperature. It is a quite difficult task to characterize the heat transfer characteristics in

the EHC in various geometric and operating conditions due to the complicated internal structure of the EHC.

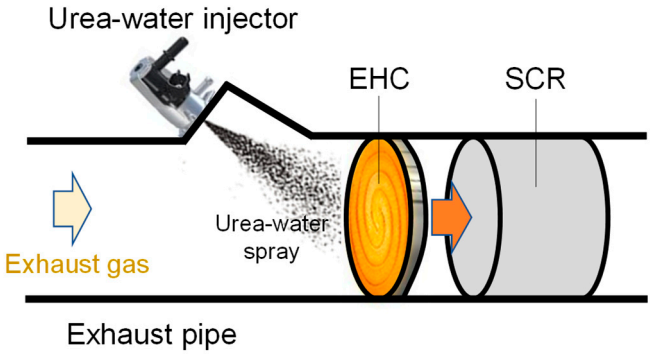

Figure 1. Illustration of EHC-based diesel urea-SCR system.

Applying the three-dimensional (3D) computational fluid dynamics (CFD) can be considered to perform this kind of flow and heat transfer analysis in the EHC, but there are some challenges to applying the CFD. First, CFD is time-consuming and expensive, particularly for the flow analysis in complicated fine structures, since it requires extremely small grid sizes to resolve the physical phenomena. Second, it is difficult to select and combine the proper models since too many parameters are engaged in the models, so the verification and calibration of model prediction results are troublesome. Last, it is difficult to investigate the effects of various geometric and operation parameters in a systematic and efficient way, which is needed for the model-based design and control of the EHC. In that sense, simplified one-dimensional (1D) theoretical models can be suitable for that purpose if the prediction accuracy of the models is acceptable. The 1D modeling works have been performed previously for the EHC system coupled with a three-way catalyst (TWC) in gasoline engines [11–13]. However, the studies mostly focused on the analysis of the catalyst temperature distribution inside the TWC, not in the EHC. The EHC has been regarded merely as a heat source for the TWC. Up to now, little attention has been paid to analyzing the thermal conditions in the EHC, which exert a critical impact on the evaporation and thermal decomposition of urea–water droplets, particularly in EHC-based urea-SCR systems adopting the direct injection of a urea–water solution to the EHC.

The current study introduces a 1D analysis scheme to characterize the heater surface temperature distribution in the EHC in various EHC geometric and operating conditions such as the flow cell diameter and length of the EHC, electrical power supply to the EHC, and exhaust gas temperature and flow rate in the EHC inlet. The energy conservation and conventional theories of forced internal convection are employed as base models for the 1D analysis with assumptions of steady-state operation, uniform heat flux from the heater to the exhaust gas, negligible thermal resistance of the heater, and constant fluid properties [28,29]. To implement the analytical approaches to the EHC with complicated structures, a tiny flow cell in the EHC is extracted for the analysis. The analyzed surface temperature results at the EHC outlet are compared with the measurement results to validate the adequacy of the analysis platform and the accuracy of prediction results. Then, the effects of various geometric parameters and operating conditions on the surface temperature distribution in the EHC are analyzed and discussed. The originality of the current study lies in the introduction of an analysis scheme to characterize the thermal conditions inside the EHC in a systematic and efficient way, and the analysis and discussion of the effects of geometric and operation parameters on the thermal conditions in the EHC that have not been thoroughly investigated in previous studies.

2. Theory and Analysis

2.1. Structure of EHC in Urea-SCR System

The picture of EHC applied in this study is presented in Figure 2. Two types of heater foils having different curvature radii are applied so that the foils can be laminated with the formation of tiny flow cells in the EHC. In general, the EHC is installed in front of the SCR and heats up the exhaust gas. The urea–water solution is also injected directly into the heater so that the thermal energy in the heater can be transferred through the heater surface for the promotion of urea–water evaporation and thermal decomposition. The EHC has an outer diameter (D_{EHC}) and is covered by the EHC housing. Each flow cell in the EHC has a cross-sectional perimetric length (blue dotted line). The equivalent diameter of a circle having the same perimetric length is defined as D_{cell}. The applied geometrical dimensions of the EHC for the 1D analysis and measurement are presented in the following sections.

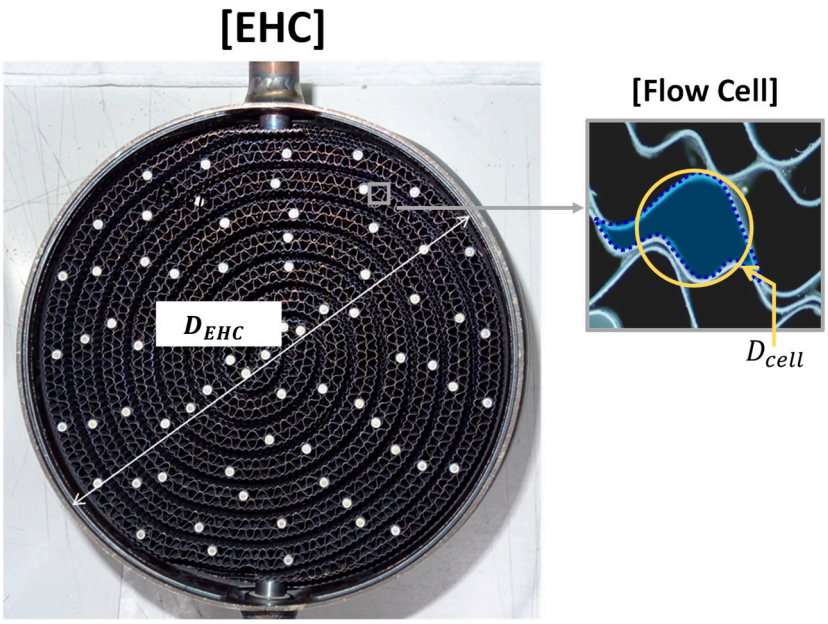

Figure 2. Structure of EHC in urea-SCR system.

2.2. 1D Analysis Models and Scheme

As mentioned in the Introduction, the application of 3D CFD is not effective in analyzing the effects of various geometric and operation parameters in a systematic way or accommodating the results to the model-based design and control. As an alternative, a 1D analysis scheme is introduced in the current study by extracting a flow cell in the EHC. The 1D analysis is based on energy conservation and the theories of forced internal convective heat transfer [28,29].

Figure 3 presents the conceptual illustration and parameters governing the flow and surface temperature distribution of a flow cell in the EHC. In the diagram, $\dot{m}_{g,cell}$ and $\dot{Q}_{cell}$ denote the mass flow rate of the gas flow to the cell and the heat transfer rate from the heater to the gas flow. $T_{g,i}$ and $T_{g,o}$ denote the cross-section-averaged gas temperature at the EHC inlet and outlet, and $T_g(x)$ denotes the exhaust gas temperature at a certain distance from the EHC inlet (x). In a similar fashion, $T_{s,i}$ and $T_{s,o}$ denote the heater surface temperature at the EHC inlet and outlet. D_{cell} and L_{cell} are geometric parameters, denoting the diameter and length of the flow cell.

The system is assumed to be operated in a steady state. Four-stroke diesel engines have intake, compression, power, and exhaust stroke in an engine cycle, and the exhaust gas flows the EHC only during the exhaust stroke [28]. However, the engines have a few cylinders (normally four) which experience the exhaust stroke in turn. Thus, the exhaust gas would flow the EHC near continuously so that the flow conditions can be regarded as

a steady state. Based on energy conservation, the total heat transfer rate to the gas ($\dot{Q}_{cell}$) can be expressed as Equation (4) with the assumption of constant specific heat, where $c_{p,g}$ denotes the constant pressure specific heat of the gas [28].

$$\dot{Q}_{cell} = \dot{m}_{g,cell} c_{p,g} (T_{g,o} - T_{g,i}) \tag{4}$$

The heat flux into the gas ($\dot{q}_{cell}$) is defined as Equation (5), which can be assumed to be uniform throughout the cell.

$$\dot{q}_{cell} = \frac{\dot{Q}_{cell}}{\pi D_{cell} L_{cell}} \tag{5}$$

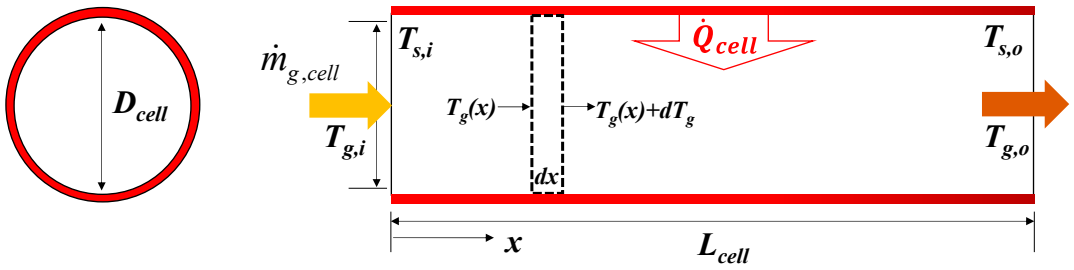

Figure 3. Conceptual illustration showing the governing parameters of flow and heat transfer in a flow cell for the 1D analysis.

This assumption can be adequate based on the steady-state consideration because the heat generated by the heater foil is spatially uniform and the heater foil thickness is sufficiently thin (around 0.1 mm) so that the conductive thermal resistance is sufficiently small to apply the lumped capacitance approach [29]. Thus, the generated heat can be regarded as all transferred to the exhaust gas through the upper and lower surfaces of the heater foil. The actual heat transfer rate and heat flux from the heater to the gas in a flow cell against the total electric power supplied to the EHC can be obtained using a scaling method in the following section.

The heat transfer rate ($d\dot{Q}$) to a differential control volume (dotted region in Figure 3) can be expressed as Equation (6).

$$\begin{aligned} d\dot{Q} &= \dot{q}_{cell} \pi D_{cell} dx \\ &= \dot{m}_{g,cell} c_{p,g} \left[(T_g(x) + dT_g) - T_g(x) \right] = \dot{m}_{g,cell} c_{p,g} dT_g(x) \end{aligned} \tag{6}$$

Then, $T_g(x)$ can be expressed as Equation (7) by solving the differential equation in Equation (6) with the boundary condition: $T_g(x)$ is $T_{g,i}$ at $x = 0$.

$$T_g(x) = \frac{\dot{q}_{cell} \pi D_{cell}}{\dot{m}_{g,cell} c_{p,g}} x + T_{g,i} \tag{7}$$

On the other hand, the heater surface temperature at x locations ($T_s(x)$) can be expressed as Equation (8) based on Newton's cooling law, where $h_g(x)$ denotes the convective heat transfer coefficient at different x locations.

$$T_s(x) = \frac{\dot{q}_{cell}}{h_g(x)} + T_g(x) \tag{8}$$

By putting the $T_g(x)$ in Equation (7) to Equation (8), $T_s(x)$ can be expressed in the form of Equation (9).

$$T_s(x) = \frac{\dot{q}_{cell} \pi D_{cell}}{\dot{m}_{g,cell} c_{p,g}} x + \frac{\dot{q}_{cell}}{h_g(x)} + T_{g,i} \tag{9}$$

Equation (9) is a traditional equation of forced internal convection of circular tubes with a constant heat flux [29]. Although the equation itself is not novel, the critical research issue raised here is how to implement this traditional equation to the specific cases of the EHC.

In the practical operation of EHC in diesel engines, the known factors are the volumetric flow rate of the exhaust gas and electrical power supply to entire EHC ($\dot{V}_{g,EHC}$ and $\dot{Q}_{EHC}$), not those to individual flow cells. $\dot{V}_{g,EHC}$ is proportional to the engine displacement volume and speed. The gas mass flow rate to the EHC ($\dot{m}_{g,EHC}$) can be obtained by multiplying the exhaust gas density (ρ_g) to $\dot{V}_{g,EHC}$. Then, $\dot{m}_{g,cell}$ can be obtained based on the known factors using Equations (10)–(12) with the assumption of constant ρ_g and $c_{p,g}$.

$$\dot{m}_{EHC} = \rho_g A_{EHC} U_g \tag{10}$$

$$\dot{m}_{cell} = \rho_g A_{cell} U_g \tag{11}$$

$$\dot{m}_{cell} = \frac{A_{cell}}{A_{EHC}} \dot{m}_{EHC} \tag{12}$$

where A_{EHC} and A_{cell} denote the cross-sectional flow area of entire EHC and flow cell, respectively. U_g denotes the gas flow velocity in the EHC inlet. Then, the $\dot{Q}_{cell}$ can also be obtained in a similar fashion using Equations (13)–(15).

$$\dot{Q}_{EHC} = \dot{m}_{g,EHC} c_{p,g} (T_{g,o} - T_{g,i}) \tag{13}$$

$$\dot{Q}_{cell} = \dot{m}_{g,cell} c_{p,g} (T_{g,o} - T_{g,i}) \tag{14}$$

$$\dot{Q}_{cell} = \frac{\dot{m}_{g,cell}}{\dot{m}_{g,EHC}} \dot{Q}_{EHC} = \frac{A_{cell}}{A_{EHC}} \dot{Q}_{EHC} \tag{15}$$

2.3. Applied Conditions and Analysis

Table 1 presents the applied conditions of the 1D analysis and corresponding Reynolds numbers (Re_D) and thermal entrance lengths ($x_{fd,t}$) of the flow in the flow cell. The applied EHC diameter (D_{EHC}) for the calculation is 119 mm. The flow cell diameters and lengths vary from 1 to 2.7 mm and from 20 to 100 mm, respectively. The applied gas flow rates ($\dot{V}_{EHC} = A_{EHC} U_g$) are 400, 800, and 1400 L/min, which are chosen based on the practical exhaust gas flow rates of a heavy-duty (4L) diesel engine. The exhaust gas temperatures in the EHC inlet are ranged from 373 K to 573 K by referring to the gas temperature measurement data of the target engine in front of the SCR in cold and normal operating conditions. The supplied heater powers are set to a maximum of 2 kW to limit the power consumption by the heater to be less than 3% of the engine power output. As shown in Table 1, the Re_D corresponding to the given gas temperature and flow rate conditions range from 13 to 211 (much lower than the critical value of 2300 for laminar to turbulence flow transition), indicating that the flow conditions in the EHC flow cells are laminar. In laminar flow conditions, the length of the thermal entrance region, in which the flow is not thermally fully developed, can be estimated based on Equation (16) [29].

$$x_{fd,t} = 0.05 D_{cell} \mathrm{Re}_D \mathrm{Pr} \tag{16}$$

where Pr denotes Prandtl number of the exhaust gas and Re_D is defined as $\mathrm{Re}_D = U_g D_{cell} / \nu_g$, where ν_g denotes the kinematic viscosity of the exhaust gas in the EHC inlet. $x_{fd,t}$ corresponding to the analysis conditions ranges from 0.4 mm to 20.3 mm (see Table 1).

Table 1. Analysis conditions.

EHC diameter (D_{EHC}, mm)	119
Flow cell diameter (D_{cell}, mm)	1, 2, 2.7
Flow cell length (L_{cell}, mm)	20, 50, 100
Gas flow rate ($\dot{V}_{EHC}$, L/min)	400, 800, 1200
EHC inlet gas temperature ($T_{g,i}$, K)	373~573
Heater power supply ($\dot{Q}_{EHC}$, kW)	0~2.0
Reynolds number (Re_D)	Min.: 13 (@D_{cell} = 1.0 mm, $\dot{V}_{EHC}$ = 400 L/min and $T_{g,i}$ = 573 K) Max.: 211 (@D_{cell} = 2.7 mm, $\dot{V}_{EHC}$ = 1200 L/min and $T_{g,i}$ = 373 K)
Thermal entrance length ($x_{fd,t}$, mm)	Min.: 0.4 (@D_{cell} = 1 mm, $\dot{V}_{EHC}$ = 400 L/min and $T_{g,i}$ = 573 K) Max.: 20.3 (@D_{cell} = 2.7 mm, $\dot{V}_{EHC}$ = 1200 L/min and $T_{g,i}$ = 373 K)

To obtain the heater surface temperature distribution in the EHC using Equation (9), $h_g(x)$ should be known through the entire EHC region. The results of the Nusselt number (Nu_D) presented in literature are used to obtain the $h_g(x)$ in the thermal entrance region and the fully developed region. Here, Nu_D is a non-dimensional number denoting the ratio of convective to conductive heat transfer, defined as in Equation (17).

$$Nu_D = \frac{h_g D_{cell}}{k_g} \tag{17}$$

where k_g denotes the thermal conductivity of the exhaust gas. The results of Nu_D in the thermal entrance region are brought from a reference, which obtained the Nu_D by the mathematical analysis of the nondimensionalized energy conservation equation in the laminar flow and constant heat flux conditions of circular tubes [30]. Figure 4 shows the estimated results of Nu_D presented in the reference as a function of characteristic distance from the EHC inlet (x^+), which is defined as in Equation (18).

$$x^+ = \frac{2x/D_{cell}}{\mathrm{Re}_D \mathrm{Pr}} \tag{18}$$

As shown in Figure 4, the Nu_D is infinite at $x = 0$. As the x increases, the Nu_D decreases in the thermal entrance region and converges to a constant value of 4.36 in the thermally fully developed region. This constant Nu_D in the fully developed region is also obtained by the control volume analysis of the differential energy equation in the circular tubes [29]. Based on the information of $Nu_D(x)$ in the literature, the $h_g(x)$ in the thermal entrance region can be obtained and used for the calculation of local surface temperature distribution in the EHC using Equation (9). Since the $h_g(x)$ cannot be defined at $x = 0$, the heater surface temperature in the EHC inlet ($T_{s,i}$) is obtained using the Nu_D result at $x^+ = 0.002$ in the following.

2.4. Potential Error Sources

The errors of 1D analysis results can occur from the undesired heat losses from the EHC to surroundings.

The heat losses from the EHC to the surroundings can occur because of convective and radiative heat transfer from the EHC housing to the surrounding air ($\dot{Q}_{ha,conv}$ and

$\dot{Q}_{ha,rad}$). The net heat energy supplied to the EHC ($\dot{Q}_{EHC,net}$) then can be estimated using Equation (19).

$$\begin{aligned}\dot{Q}_{EHC,net} &= \dot{Q}_{EHC} - \dot{Q}_{ha,conv} - \dot{Q}_{ha,rad} \\ &= \dot{Q}_{EHC} - h_{ha}A_{hs}(T_{hs} - T_a) - \varepsilon_{ha}\sigma A_{hs}({T_{hs}}^4 - {T_a}^4)\end{aligned} \quad (19)$$

where h_{ha}, ε_{ha}, A_{hs}, and T_{hs} denote the convective heat transfer coefficient between the EHC housing and air and the emissivity, surface area, and temperature of EHC housing at its outer surface, respectively. However, in the current analysis, the heat losses are not considered for the calculation because the T_{hs} is sufficiently low due to the high thermal resistance of the housing material and the existence of an air gap (an effective insulator) between the heater and housing. The adequacy of this simplification is discussed by the measurement results of EHC surface temperature and model validation in the following sections.

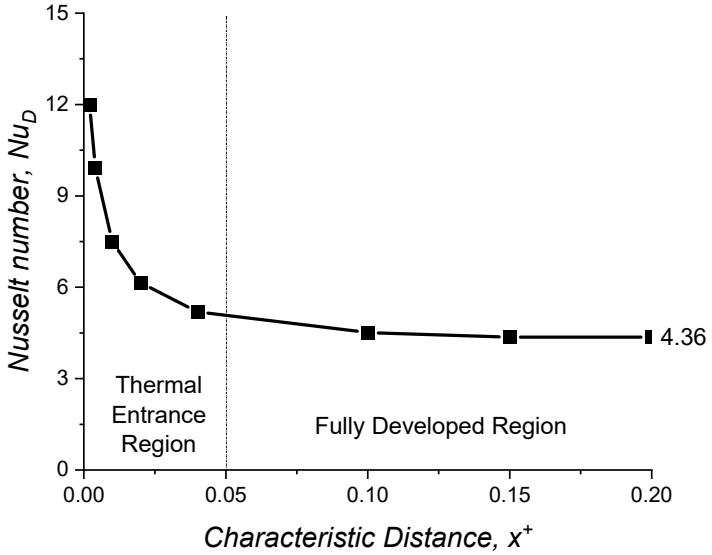

Figure 4. Nusselt number of laminar flows inside circular tubes in the thermal entrance region [30].

3. Measurements

Experiments were performed to measure the heater surface temperature distribution at the EHC outlet ($T_{s,o}$), and a picture of the experimental setup is presented in Figure 5a. Simulated exhaust gases were generated by the ultra-lean combustion of liquified petroleum gas (LPG). The LPG was used for the generation of exhaust gas to control the exhaust gas flow rate and temperature with more ease because with the premixed combustion, it is easier to control those parameters. The premixed LPG combustion was performed in a constant volume chamber to control those parameters by varying the supplying flow rates and equivalence ratio of the LPG–air mixture in the chamber. The exhaust gas temperatures were measured in front of the EHC using a thermocouple. The heater surface temperature distributions were measured in the EHC outlet using an infrared (IR) camera (FLIR Systems Co., Ltd., Wilsonville, OR, USA, THermaCAM S65) after the surface temperature reaches a steady-state condition. Unfortunately, the surface temperature distribution at the EHC inlet is not measurable because the EHC inlet is invisible due to the existence of an exhaust pipe. The temperature measurement results of the IR camera at four locations of the EHC outlet (black cross-marks in Figure 5b) were averaged to obtain the representative temperature result at each condition.

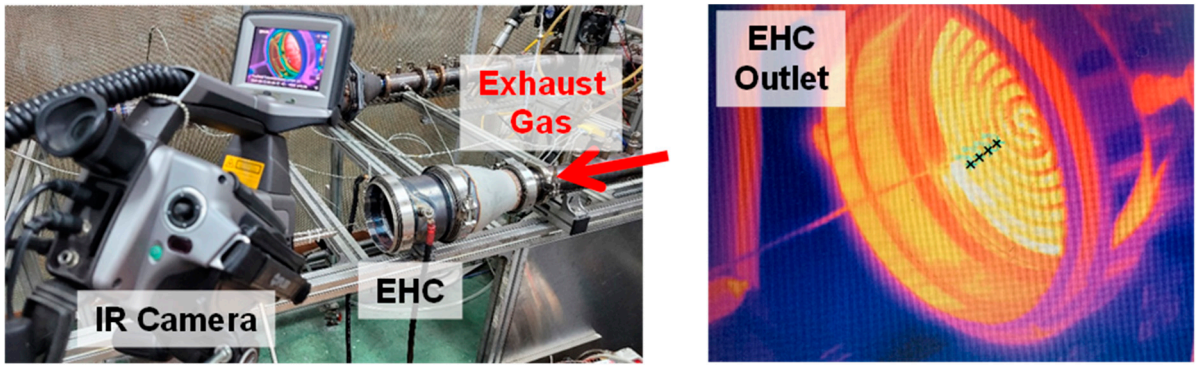

(**a**) (**b**)

Figure 5. Picture of experimental setup for the measurement of heater surface temperature at the EHC outlet (**a**) and the locations of temperature measurement (**b**).

Table 2 shows the measurement conditions of heater surface temperature at the EHC outlet. The measurement variables are $\dot{Q}_{EHC}$, $\dot{V}_{EHC}$, and $T_{g,i}$. Due to the control difficulties of $\dot{V}_{EHC}$ and $T_{g,i}$ from the simulated exhaust gases, the measurements were performed in limited conditions. The D_{cell} and L_{cell} of the EHC used for the measurement were 2.7 mm and 20 mm, respectively. The L_{cell} of 20 mm was chosen to estimate the validity of model prediction results in the marginal condition in which the effect of $x_{fd,t}$ might appear (see $x_{fd,t}$ for each condition in Table 2). The data are used for the model validation, and the results are presented in the following section.

Table 2. Measurement conditions of surface temperature at the EHC outlet.

D_{cell} (mm)	L_{cell} (mm)	$\dot{Q}_{EHC}$ (kW)	$\dot{V}_{EHC}$ (L/min)	$T_{g,i}$ (K)	Re_D	$x_{fd,t}$ (mm)
2.7	20	0.04	800	513	61.4	5.8
		0.17		533	57.6	5.4
		0.38				
		0.67	1400	445	182	17.2
		1.00				
		1.47				
		2.00		501	149	14.0

The local average and deviation results of $T_{s,o}$ measured using the IR camera are presented in Figure 6. The results show that the local deviation of $T_{s,o}$ is a maximum of 8.64% in the measurement conditions, which demonstrates the local uniformity of $T_{s,o}$. This near-uniform surface temperature distribution can be from the uniform heat generation of the heater and the negligible stray heat transfer from the EHC to the surroundings. It implies that the current analysis scheme and model simplifications are adequate.

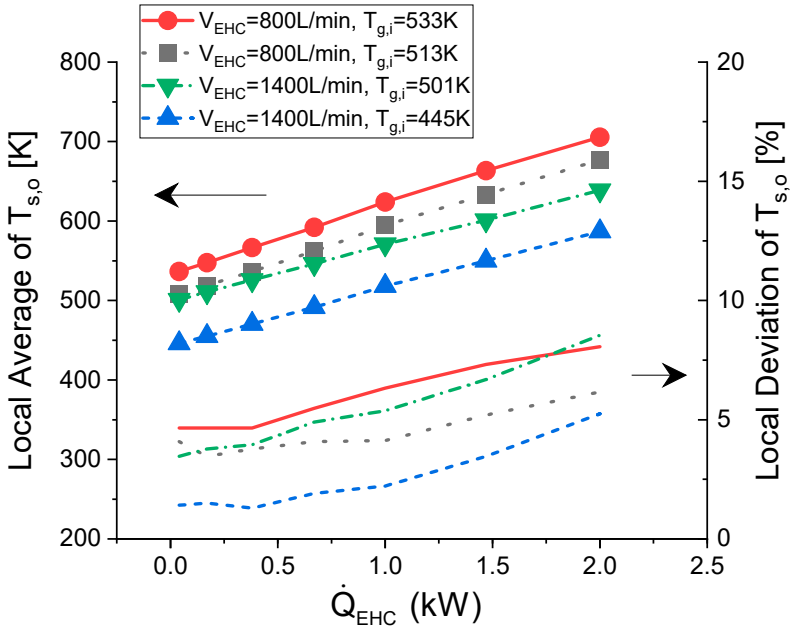

Figure 6. Local average and deviation results of $T_{s,o}$ measured using IR camera.

4. Results and Discussion

In this section, the adequacy of 1D prediction results is discussed first by comparing them with the measurement results. Then, the effects of EHC geometric (D_{cell} and L_{cell}) and operation parameters ($\dot{V}_{EHC}$, $T_{g,i}$ and $\dot{Q}_{EHC}$) on T_s distribution in the EHC are presented and discussed based on the 1D analysis results.

4.1. Validation of 1D Analysis Results

Figure 7 compares the prediction and measurement results of $T_{s,o}$ in the conditions given in Table 2. The error rates of the prediction results are also presented. For the simplicity of 1D model analysis, the properties of exhaust gases are assumed as those of air since the properties of simulated exhaust gases are quite close to those of air in the ultra-lean combustion conditions (maximum 3%, 8%, and 7% difference in Pr, k, and ρ in given flow conditions).

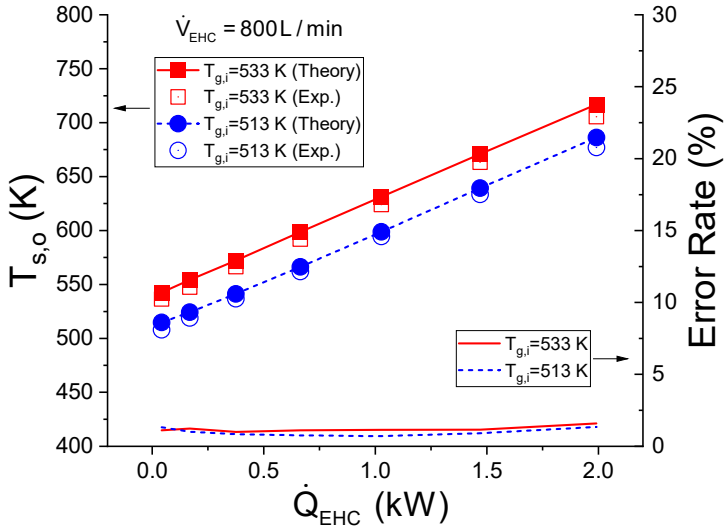

(**a**)

Figure 7. *Cont.*

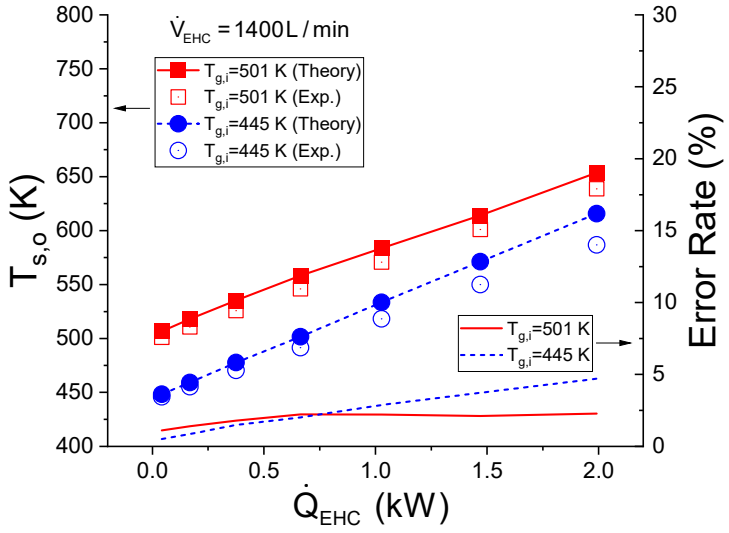

(**b**)

Figure 7. Comparison of predicted and measured surface temperature results at the EHC outlet ($T_{s,o}$) under various exhaust gas flow rates ($\dot{V}_{EHC}$) and temperatures ($T_{g,i}$), and supplied heater powers ($\dot{Q}_{EHC}$): (**a**) $\dot{V}_{EHC}$ = 800 L/min, (**b**) $\dot{V}_{EHC}$ = 1400 L/min (D_{cell} = 2.7 mm, L_{cell} = 20 mm).

The results show that, in general, the predicted $T_{s,o}$ from the 1D model matches quite well with the measurement results, but the error rate increases with the increase in $\dot{Q}_{EHC}$, especially at the high flow rate condition (see Figure 7b). The increased error at the high $\dot{Q}_{EHC}$ condition can result from the increased heat loss to the surroundings due to the higher temperature of the EHC and housing. However, the error rates in the applied conditions are limited to a maximum of 5%, which indicates that the 1D analysis scheme suggested in the current study has over 95% reliability in the operating conditions of the 4L class heavy-duty diesel engine. This reliability would increase further for the smaller engines in which exhaust gas flow rates and maximum applicable heater powers are lower.

4.2. Effects of EHC Geometric Parameters on Surface Temperature Distributions

Based on the proven reliability, the effects of EHC geometric parameters such as D_{cell} and L_{cell} on the surface temperature distribution are discussed based on the 1D analysis results.

Figure 8a presents the effect of D_{cell} on the surface temperature distribution in the EHC. The results in a fixed condition of the other parameters ($\dot{V}_{EHC}$ = 800 L/min, $T_{g,i}$ = 473 K, $\dot{Q}_{EHC}$ = 2 kW, L_{cell} = 50 mm) are only presented here since the results trend of D_{cell} effect appears equivalent regardless of the condition. The results show that D_{cell} does not affect the slope of the surface temperature with x in the fully developed condition. As shown in Equation (9), the slope of $T_s(x)$ is linearly dependent on $\dot{q}_{cell}D_{cell}/\dot{m}_{g,cell}$. $\dot{m}_{g,cell}$ has a linear relationship with A_{cell}, which is proportional to the square of D_{cell}. Based on Equation (5), $\dot{q}_{cell}$ is proportional to D_{cell} because $\dot{Q}_{cell}$ is proportional to the square of D_{cell}, as shown in Equation (15). Thus, the slope of $T_s(x)$ in Equation (9) becomes independent of D_{cell}. On the other hand, T_s-intercept in Equation (9) increases upon the increase in D_{cell} since $\dot{q}_{cell}$ is proportional to D_{cell}. As a result, the larger D_{cell} causes a higher $T_s(x)$ in the fully developed region. However, the increase in $T_s(x)$ is only around 40 K even with a nearly 3 times larger D_{cell}. The effect of D_{cell} on $T_{s,i}$ is insignificant due to the substantially high h_g in the inlet ($x \cong 0$), although the $\dot{q}_{cell}$ increases linearly upon the increase in D_{cell} (see Equation (9)).

Figure 8b presents the effect of L_{cell} on the surface temperature distribution in the EHC. Only the results in a fixed condition of the other parameters ($\dot{V}_{EHC}$ = 800 L/min,

$T_{g,i}$ = 473 K, $\dot{Q}_{EHC}$ = 2 kW, D_{cell} = 2.7 mm) are presented. The results show that the slope of $T_s(x)$ decreases with the increase in L_{cell} because the $\dot{q}_{cell}$, the only factor affecting the slope in Equation (9), is inversely proportional to L_{cell}, as shown in Equation (5). The decrease in the slope and $\dot{q}_{cell}$ causes the lower T_s at longer L_{cell} in all regions of the EHC. Again, the effect of L_{cell} on $T_{s,i}$ is insignificant due to the substantially high h_g in the inlet ($x \cong 0$).

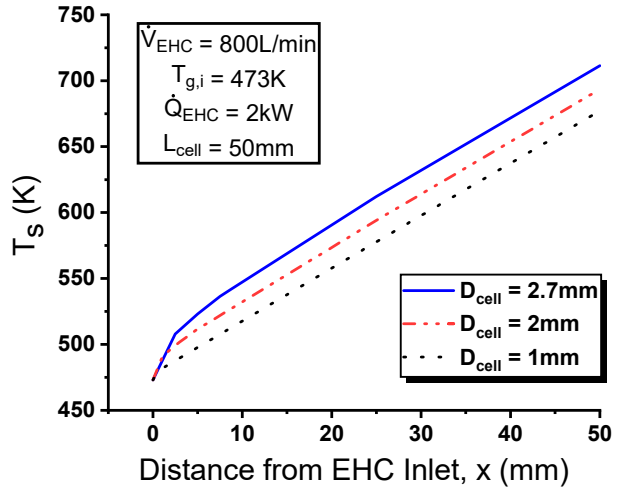

(**a**)

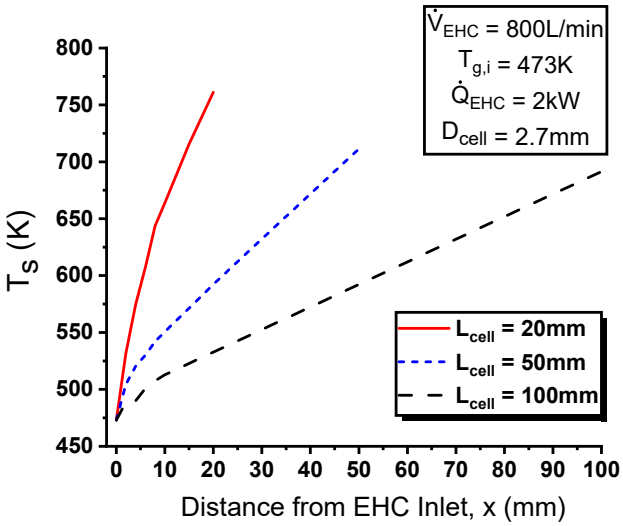

(**b**)

Figure 8. Effect of flow cell diameter (D_{cell}) and length (L_{cell}) on the surface temperature distribution in the EHC: (**a**) effect of D_{cell}, (**b**) effect of L_{cell}.

Overall, the effect of L_{cell} appears to be much more critical on the surface temperature distribution compared to that of D_{cell}. The most relevant factor associated with this result trend is $\dot{q}_{cell}$, which represents the heat generation potential of the heater material. The results indicate that reducing the L_{cell} can be effective to increase the heater surface temperature in the fixed $\dot{Q}_{EHC}$ and $\dot{V}_{EHC}$ conditions. However, it should be confirmed when applying the short L_{cell} if the heater material has sufficient durability against the high heat load.

4.3. Effects of Operation Parameters on Surface Temperature Distributions

The effects of operation parameters such as $\dot{V}_{EHC}$, $T_{g,i}$, and $\dot{Q}_{EHC}$ on surface temperature distribution in the EHC are investigated for the EHC with D_{cell} of 2.7 mm and L_{cell}

of 20 mm. Figure 9a presents the effect of $\dot{V}_{EHC}$ and $\dot{Q}_{EHC}$ on $T_{s,i}$ and $T_{s,o}$ in the fixed $T_{g,i}$ of 523 K. The $T_{s,i}$ is not varying with $\dot{V}_{EHC}$ because the T_s-intercept in Equation (9) is independent of $\dot{V}_{EHC}$. On the other hand, the $T_{s,o}$ decreases with the increase in $\dot{V}_{EHC}$ because the slope in Equation (9) is inversely proportional to $\dot{V}_{EHC}$ (or $\dot{m}_{EHC}$). The larger $\dot{Q}_{EHC}$ causes the higher $T_{s,i}$ and $T_{s,o}$, but the degree of increase appears much larger for $T_{s,o}$. Figure 9b presents the effect of $T_{g,i}$ and $\dot{Q}_{EHC}$ on $T_{s,i}$ and $T_{s,o}$ in the fixed $\dot{V}_{EHC}$ of 800 L/min. The higher $T_{g,i}$ increases both $T_{s,i}$ and $T_{s,o}$, and the increase rate against $\dot{Q}_{EHC}$ appears almost identical for $T_{s,o}$ regardless of $T_{g,i}$. This is because the $T_{g,i}$ is placed in the T_s-intercept and does not affect the slope itself in Equation (9). The effect of $\dot{Q}_{EHC}$ appears in a similar fashion to that in Figure 9a.

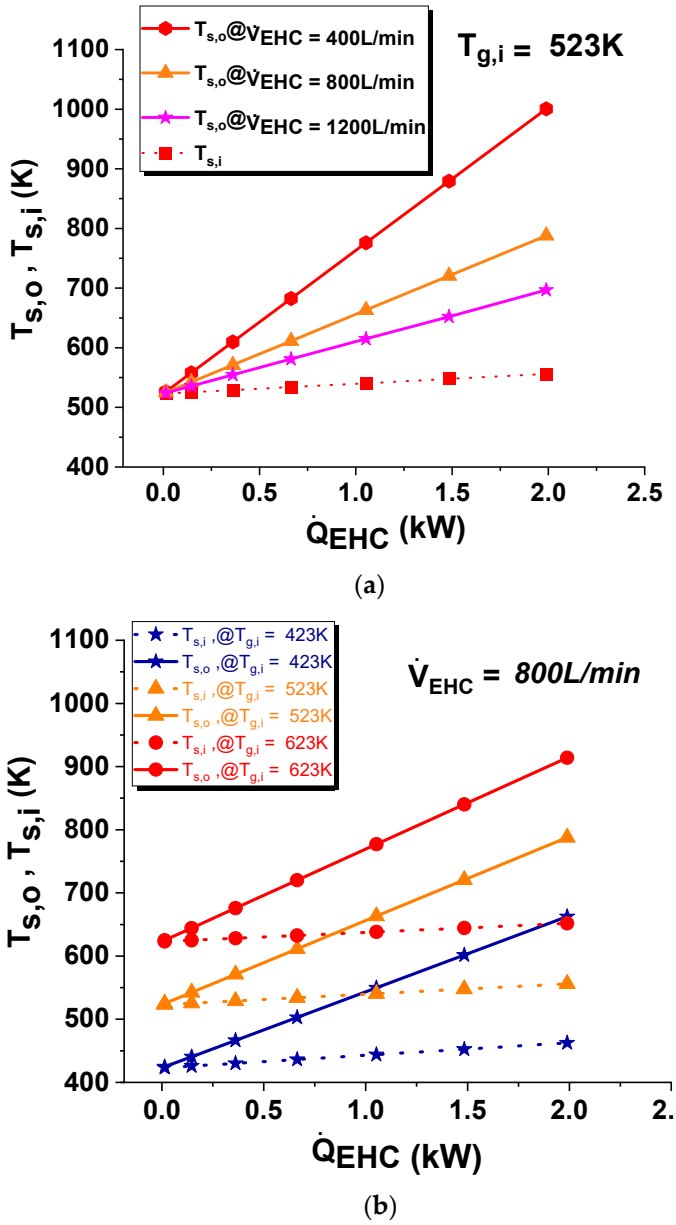

Figure 9. Effect of flow rate ($\dot{V}_{EHC}$) and temperature ($T_{g,i}$) of exhaust gas and heater power ($\dot{Q}_{EHC}$) on the heater surface temperature distribution in the EHC: (**a**) effect of $\dot{V}_{EHC}$ and $\dot{Q}_{EHC}$, (**b**) effect of $T_{g,i}$ and $\dot{Q}_{EHC}$ (D_{cell} = 2.7 mm, L_{cell} = 20 mm).

An interesting point to discuss here is that the increase in $T_{s,i}$ is not as significant as that of $T_{s,o}$ in all conditions. Even with the application of maximum allowable heater power (2 kW), the increase rate of $T_{s,i}$ is only limited to 8.5% in its maximum. It indicates that the impingement location and jet-wall interaction of urea–water injection in the EHC should be carefully designed not to place the large portion of urea–water droplets near the EHC inlet in which the evaporation of urea–water solution would be inferior, and the possibility of urea deposit formation would be high.

4.4. Discussion

In the above sections, the 1D analysis scheme characterizing the surface and exhaust gas temperature distribution in the EHC is introduced, which is based on energy conservation and conventional theories of forced internal convection. Novel approaches have been applied to extract the tiny flow cell in the EHC for the analysis and scale the gas flow rate and heater power to the flow cell based on known operation factors. Although some assumptions and simplifications are applied in the 1D analysis, the validation results show a high prediction accuracy in the operation conditions of the 4L diesel engine. The prediction accuracy of this analysis scheme would be further guaranteed for the smaller size engines. Even for the larger size engines, the analysis scheme can be used, but the effect of different flow conditions should be considered because the flow rate ($\dot{V}_{EHC}$) can become higher and the flow cell diameter (D_{cell}) can become larger. In that case, the flow condition can be changed to turbulent due to the larger Re_D. Even in the turbulent flow conditions, the same analysis scheme can be applied, but the $h_g(x)$ should be newly defined. The Dittus–Boelter equation presented in Equation (20) or the other correlations can be used to define the Nu_D in the turbulent flow conditions [31,32].

$$Nu_D = 0.023\mathrm{Re}_D{}^{0.8}\mathrm{Pr}^{0.4} \tag{20}$$

The 1D analysis scheme can analyze the effect of various geometric and operation parameters on the thermal conditions in the EHC in a systematic and efficient way. The operation map can be built shortly based on the 1D analysis scheme that can be used to determine the optimized $\dot{Q}_{EHC}$ condition in various operating conditions to accomplish the complete evaporation and decomposition of the urea–water solution, and to avoid the formation of urea deposit. For that purpose, the 1D analysis scheme can also be coupled with the prediction models of evaporation and decomposition of the urea–water solution, and urea deposit formation.

5. Conclusions

In this study, a 1D analysis scheme based on the energy conservation and theories of forced internal convection was introduced to characterize the surface temperature distribution in the electrically heated catalyst (EHC) for urea-based selective catalytic converter (SCR) systems. A fine flow cell in the EHC was extracted for the 1D heat transfer analysis with some assumptions and simplifications. The gas flow rate and heater power supply to the flow cell were scaled based on information of those to the entire EHC region. The 1D prediction results were validated using the surface temperature measurement results at the EHC outlet in simulated conditions of a heavy-duty diesel engine. Based on the proven reliability of 1D prediction results, the effects of various EHC geometric and operation parameters on the surface temperature distribution in the EHC were analyzed and discussed. The key findings and discussion points of the current study are summarized below.

1. The flows in the flow cell were found to be laminar in given EHC operating and geometric conditions. The measurement results showed near-uniform surface temperature distributions at the EHC outlet (maximum 8.64% local deviation), which demonstrated the adequacy of the current analysis scheme extracting a fine flow cell

in the EHC for the analysis. The prediction results showed over 95% accuracy in the given engine conditions.

2. The 1D analysis results showed that the surface temperature increased with the enlarged flow cell diameter and the reduced EHC length in the fixed gas flow rate and heater power conditions of the EHC. The increase in the EHC heater power caused the higher surface temperature in both the EHC inlet and outlet, but the temperature increase rate was much less in the EHC inlet. Increasing the exhaust gas flow rate reduced the surface temperature while increasing the exhaust gas temperature caused a higher EHC surface temperature.

The main contribution of this work is the introduction of an analysis scheme to characterize the thermal conditions inside the EHC in a systematic and efficient way. The current analysis scheme showed high prediction accuracy in the operating conditions of a heavy-duty diesel engine, and its application can be extended to larger size engines that would have turbulent flows in the EHC.

Author Contributions: S.M.: Conceptualization, Investigation, Methodology, Writing—original draft preparation, Supervision, Funding acquisition. S.P.: Data curation, Methodology, Formal analysis, Investigation, Visualization. J.S.: Methodology, Formal analysis, Investigation, Visualization. K.O.: Investigation, Resources, Funding acquisition. S.J.: Resources, Project administration. All authors have read and agreed to the published version of the manuscript.

Funding: This work was supported by Korea Environment Industry & Technology Institute (KEITI) through the Reduction Management Program of Fine Dust Blind-Spots, funded by Korea Ministry of Environment (MOE) (grant no. 2020003060011).

Conflicts of Interest: The authors declare that they have no known competing financial interest or personal relationships that could have appeared to influence the work reported in this paper.

References

1. CARB Developing Tier 5 Emission Standards for Off-Road Engines. Available online: https://dieselnet.com/news/2021/11carb.php (accessed on 1 April 2022).
2. Kim, D.S.; Wang, T.J. Diesel Engine Technologies for Next-generation Stage V Emission Regulation. *KSAE Auto J.* **2017**, *39*, 25–30.
3. Selective Catalytic Reduction. Available online: https://dieselnet.com/tech/cat_scr.php (accessed on 1 April 2022).
4. Bornhorst, M.; Deutschmann, O. Advances and challenges of ammonia delivery by urea-water sprays in SCR systems. *Prog. Energy Combust. Sci.* **2021**, *87*, 100949. [CrossRef]
5. Liu, S.; Wang, B.; Guo, Z.; Wang, B.; Zhang, Z.; Ma, X.; Chang, C.; Wang, P.; He, X.; Sun, X.; et al. Experimental investigation of urea injection strategy for close-coupled SCR aftertreatment system to meet ultra-low NOx emission regulation. *Appl. Therm. Eng.* **2022**, *25*, 117994.
6. Prabhu, S.; Natesan, K.; Nayak, N.S. Effect of UWS spray angle and positioning of injector on ammonia concentration in Urea-SCR system. *Mater. Today Proc.* **2021**, *46*, 8051–8055. [CrossRef]
7. Pratama, R.H.; Moon, S.; Kim, H.; Oguma, M. Application of electrostatic force for the atomization improvement of urea-water sprays in diesel SCR systems. *Fuel* **2020**, *262*, 116571. [CrossRef]
8. Ju, K.; Hong, J.; Park, C. Effect of Assist-air of Twin Fluid Atomizer on Urea Thermal Decomposition. *At. Sprays* **2015**, *25*, 895–915.
9. Miao, Y.; Chen, L.; He, Y.; Kuo, T. Study of SCR cold-start by energy method. *Chem. Eng. J.* **2009**, *155*, 260–265. [CrossRef]
10. Lee, Y.; Lee, S.; Lee, S.; Choi, H.; Min, K. Characteristics of NOx emission of light-duty diesel vehicle with LNT and SCR system by season and RDE phase. *Sci. Total Environ.* **2021**, *782*, 146750. [CrossRef]
11. Bezaire, B.A. Modeling and Control of an Electrically-Heated Catalyst. Master's Thesis, The Ohio State University, Columbus, OH, USA, 2011.
12. Ning, J.; Yan, F. Temperature Control of Electrically Heated Catalyst for Cold-start Emission Improvement. *IFAC-PapersOnLine* **2016**, *49*, 14–19. [CrossRef]
13. Velmurugan, D.V.; McKelvey, T.; Olsson, J. A simulation framework for cold-start evaluation of a gasoline engine equipped with an electrically heated three-way catalyst. *IFAC-PapersOnLine* **2021**, *54*, 14–19. [CrossRef]
14. Gao, J.; Tian, G.; Sorniotti, A. On the emission reduction through the application of an electrically heated catalyst to a diesel vehicle. *Energy Sci. Eng.* **2019**, *7*, 2383–2397. [CrossRef]
15. Nazir, M.T.; Brammer, M.; Scholz, R.; Zote, F.; Bunar, F.; Schrade, F. Electrically Heated Catalyst (EHC) Development of Diesel Applications. *Int. J. Automot. Eng.* **2015**, *6*, 127–133.
16. Kim, C.H.; Paratore, M.; Gonze, E.; Solbrig, C.; Smith, S. *Electrically Heated Catalysts for Cold-Start Emissions in Diesel Aftertreatment*; SAE Technical Paper 2012-01-1092; SAE International: Warrendale, PA, USA, 2012.

17. Lee, S.H.; Lee, K.B.; Won, J.H.; Lee, J.G.; Oh, K.W. An Experimental Study on the effect of Urea-SCR doing system using EHC on NOx reduction. In Proceedings of the 2021 KSAE (The Korean Society of Automotive Engineers) Fall Conference, Yeosu, Korea, 17–20 November 2021; pp. 118–119.
18. Wang, T.J.; Baek, S.W.; Lee, S.Y. Experimental Investigation on Evaporation of Urea-Water-Solution Droplet for SCR Applications. *AIChE J.* **2009**, *55*, 3267–3276. [CrossRef]
19. Wei, L.; Youtong, Z.; Asif, M. Investigation on UWS Evaporation for Vehicle SCR Applications. *AIChE J.* **2016**, *62*, 880–890. [CrossRef]
20. Grout, S.; Blaisot, J.; Pajot, K.; Osbat, G. Experimental investigation on the injection of an urea–water solution in hot air stream for the SCR application: Evaporation and spray/wall interaction. *Fuel* **2013**, *106*, 166–177. [CrossRef]
21. Ebrahimian, V.; Nicolle, A.; Habchi, C. Detailed Modeling of the Evaporation and Thermal Decomposition of Urea-Water Solution in SCR Systems. *AIChE J.* **2012**, *58*, 1998–2009. [CrossRef]
22. Kuntz, C.; Kuhn, C.; Weickenmeier, H.; Tischer, S.; Börnhorst, M.; Deutschmann, O. Kinetic modeling and simulation of high-temperature by-product formation from urea decomposition. *Chem. Eng. Sci.* **2021**, *246*, 116876. [CrossRef]
23. Nishad, K.; Stein, M.; Ries, F.; Bykov, V.; Maas, U.; Deutschmann, O.; Janicka, J.; Sadiki, A. Thermal Decomposition of a Single AdBlue® Droplet Including Wall–Film Formation in Turbulent Cross-Flow in an SCR System. *Energies* **2016**, *12*, 2600. [CrossRef]
24. Yim, S.; Kim, S.; Baik, J.; Nam, I.; Mok, Y.; Kee, J.; Cho, B.; Oh, S. Decomposition of Urea into NH3 for the SCR Process. *Ind. Eng. Chem. Res.* **2004**, *43*, 4856–4863. [CrossRef]
25. Smith, H.; Lauer, T.; Mayer, M. *Optical and Numerical Investigations on the Mechanisms of Deposit Formation in SCR Systems*; SAE Technical Paper 2014-01-1563; SAE International: Warrendale, PA, USA, 2014.
26. Schiller, S.; Brandl, M.; Hoppenstedt, B.; Rudder, K.D. *Wire Mesh Mixer Optimization for DEF Deposit Prevention*; SAE Technical Paper 2015-01-0989; SAE International: Warrendale, PA, USA, 2015.
27. Weeks, C.L.; Ibeling, D.R.; Han, S.; Ludwig, L.; Ayyappan, P. *Analytical Investigation of Urea Deposits in SCR System*; SAE Technical Paper 2015-01-1037; SAE International: Warrendale, PA, USA, 2015.
28. Moran, M.J.; Shapiro, H.N.; Boettner, D.D.; Bailey, M.B. *Principles of Engineering Thermodynamics*; Global Edition; John Wiley & Sons Inc.: Singapore, 2017.
29. Incropera, F.P.; Dewitt, D.P.; Bergman, T.L.; Lavine, A.S. *Incropera's Principle of Heat and Mass Transfer*; Global Edition; John Wiley & Sons Inc.: Singapore, 2017.
30. Kays, W.M.; Crawford, M.E.; Weigand, B. *Convective Heat and Mass Transfer*, 4th ed.; McGraw-Hill: Boston, MA, USA, 2005.
31. Dittus, F.W.; Boelter, L.M.K. Heat transfer in automobile radiators of the tubular type. *Univ. Calif. Publ. Eng.* **1930**, *2*, 443–461. [CrossRef]
32. Winterton, R.H.S. Where did the Dittus and Boelter equation come from? *Int. J. Heat Mass Transf.* **1998**, *41*, 809–810. [CrossRef]